Dispersion relation of capillary waves on ionic liquids: Observation of the fast overdamped mode

T. Hoshino,[1] Y. Ohmasa,[2] R. Osada,[1] and M. Yao[1]
[1]*Department of Physics, Kyoto University, 606-8502 Kyoto, Japan*
[2]*Faculty of Engineering, Hiroshima Institute of Technology, 731-5193 Hiroshima, Japan*
(Received 11 September 2008; published 17 December 2008)

We measured the capillary wave spectra on the surface of ionic liquids using dynamic light scattering techniques. Empirical dispersion relations deduced from the time domain analysis clearly reveal the transition from oscillating to overdamped behavior with changing temperature and the wave vector. In particular, not only slow but also fast modes were observed in the overdamped regime. The empirical dispersion relations coincide with the theoretical dispersion relations deduced from the linearized Navier-Stokes equation when experimentally determined density, viscosity, and surface tension are assigned to the latter.

DOI: 10.1103/PhysRevE.78.061604 PACS number(s): 68.03.Kn, 47.35.Pq, 78.35.+c

I. INTRODUCTION

The liquid-vapor interface is microscopically not flat, because thermally agitated capillary waves (CWs) are generated and damped continually. Theoretical dispersion relation of CWs can be calculated from the linearized Navier-Stokes equation [1], which is dominated by the surface tension σ, viscosity η, and density ρ. Interestingly, the CWs can be either oscillating or overdamped, depending on σ, η, ρ, and the wave vector Q.

Experimental studies of the transition from oscillating to overdamped behavior of the CWs have been done by dynamic light scattering (DLS) technique. Byrne and Earnshaw [2] applied DLS to the investigation of CWs on the free surfaces of two liquids having extreme values of viscosity: water (with low viscosity) and glycerin (with high viscosity). They observed oscillating behavior on the water surface and overdamped behavior on the glycerin surface over the entire range of wave vectors investigated. A pioneering work of observing the transition from oscillating to overdamped behavior was done by Madsen *et al.* [3]. They measured the CW spectra on the surface of aqueous solution of glycerin by x-ray photon correlation spectroscopy (XPCS) and assigned the Q point where the peak position ω_m of the CW spectrum moved to zero frequency at the transition point.

In the overdamped regime, the hydrodynamic theory indicates that the CWs decay at two different rates. However, to our knowledge, the fast overdamped mode has never been observed on free liquid surfaces, though Crilly and Earnshaw [4] observed the fast overdamped mode in the interfacial capillary waves for bilayer membranes of glycerol monooleate.

Recently, ionic liquids (ILs) have received considerable interest for various applications such as solvents in chemical synthesis [5] and electrolytes in batteries [6] and solar cells [7]. The surface of ILs has been actively studied from basic points of view, and unique surface properties have been reported [8–12]. For example, at the surface of 1-alkyl-3-methylimidazolium tetrafluoroborates, a molecular layer is formed [8] and the alkyl chains of imidazolium rings protrude from the bulk liquid into the air [9].

Ohmasa *et al.* [13] measured the CW spectra on 1-butyl-3-methylimidazolium bis[(trifluoromethyl)sulfonyl]imide (hereafter abbreviated as [C_4mim][TFSI]) by DLS techniques, and observed the transition from oscillating to overdamped behavior of CWs for the first time. A remarkable achievement of their work is to describe the observed CW spectra using the fluctuation-dissipation theorem and deduce accurate values of σ and η from them in a wide temperature range. Subsequently, Sloutskin [14] *et al.* measured the CW spectra on 1-butyl-3-methylimidazolium tetrafluoroborate ([C_4mim][BF_4]) by XPCS, and investigated both the Q dependence and temperature dependence of the peak position ω_m in the frequency domain spectra. They described the behavior of ω_m by the fluctuation-dissipation theorem even in the transition region. These two works [5,14] have commonly pointed out that the presence of a dipole layer on IL, suggested by Halka *et al.* [15–17], should be ruled out.

In this paper, extending the work by Ohmasa *et al.* [13], we investigate the CW spectra of six ionic liquids (ILs), namely [C_4mim][TFSI], tetramethylammonium bis[(trifluoromethyl)sulfonyl]imide ([TMPA][TFSI]), N-methyl-N-propylpiperidinium bis[(trifluoromethyl)sulfonyl]imide ([PP13][TFSI]), and 1-alkyl-3-methylimidazolium hexafluorophosphate ([$C_n$mim][PF_6], $n=4,6,8$), by DLS measurements. ILs are suitable samples for studying the dispersion relation of CWs in the vicinity of the transition from oscillating to overdamped behavior, because the viscosity of ILs considerably changes near the room temperature and hence we can easily access the condition in which the transition occurs by adjusting temperature.

This paper is constructed as follows. We review the theoretical background of the dispersion relation of CWs in Sec. II. Experimental methods for measuring the CW spectra are explained in Sec. III. In Sec. IV, we present the dispersion relations obtained via two different routes: one is empirical dispersion relation deduced from time domain analysis, and the other is the theoretical one deduced from hydrodynamic calculations. Conclusions are drawn in Sec. V.

II. THEORETICAL BACKGROUND

The dispersion relation of CWs on a free liquid surface is briefly reviewed here. We consider the waves propagating in only the x direction on the $z=0$ plane which is a hypothetical

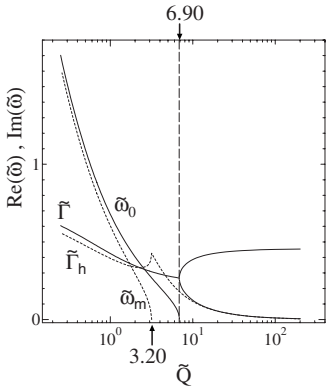

FIG. 1. Theoretical dispersion relations of capillary waves. The solid lines represent $\mathrm{Re}(\tilde{\omega})=\tilde{\omega}_0$ and $\mathrm{Im}(\tilde{\omega})=\tilde{\Gamma}$ calculated by Eq. (6), which are deduced from the linearized Navier-Stokes equation (solid lines). The dotted lines represent Q dependence of peak frequencies $\tilde{\omega}_m$ and widths $\tilde{\Gamma}_h$ of power spectra Eq. (7), which is deduced from the fluctuation-dissipation theorem.

liquid surface without CWs. The displacement $u(x,t)$ of the surface from $z=0$ can be expressed by

$$u(x,t) = u_0 \exp[i(Qx + \omega t)], \tag{1}$$

where Q is the wave vector and ω is the complex frequency.

From the hydrodynamic calculation [1], the dispersion equation of CWs is given by

$$D(Q,\omega) = 0, \tag{2}$$

where

$$D(Q,\omega) = (2\eta Q^2/\rho)^2\sqrt{1 + i\omega\rho/\eta Q^2} - (i\omega + 2\eta Q^2/\rho)^2 - \sigma Q^3/\rho. \tag{3}$$

Using the dimensionless substitutions,

$$\tilde{\omega} = \frac{\omega\rho}{2\eta Q^2}, \tag{4}$$

$$\tilde{Q} = \frac{4\eta^2 Q}{\rho\sigma}, \tag{5}$$

one can simplify Eq. (2) to the following expression:

$$(1 + 2i\tilde{\omega})^{1/2} - (1 + i\tilde{\omega})^2 - 1/\tilde{Q} = 0. \tag{6}$$

Let us describe the solution of Eq. (6) as $\tilde{\omega}=\tilde{\omega}_0+i\tilde{\Gamma}$. In Fig. 1, $\tilde{\omega}_0$ and $\tilde{\Gamma}$ are plotted as a function of $\tilde{Q}$. For $\tilde{Q} < 1/0.145 \approx 6.90$, Eq. (6) has two complex conjugate roots, but for $\tilde{Q} \geqslant 6.90$ it has two pure imaginary roots. Therefore the CWs for $\tilde{Q} < 6.90$ show a damped oscillating behavior, and the CWs for $\tilde{Q} \geqslant 6.90$ show an overdamped behavior with two different damping rates, i.e., a slow one Γ_s and a fast one Γ_f. While the slow overdamped mode mainly corresponds to a recovery motion under the shear drag, the fast one is required when the inertia effects are not ignored. Due to the large increasing rate of Γ_f with Q, the fast overdamped mode of CWs has never been experimentally observed on free liquid surfaces so far [2].

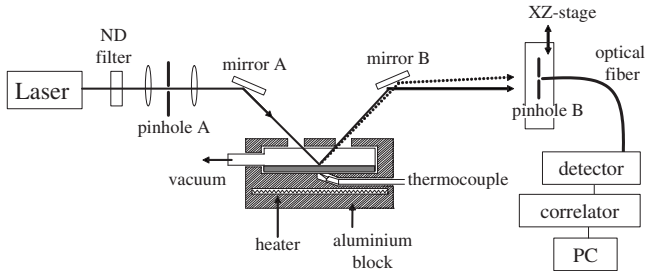

FIG. 2. Schematic drawing of the experimental setup for the surface dynamic light scattering measurements.

From the fluctuation-dissipation theorem [18,19], the power spectrum $P_T(Q,\omega)$ of thermally excited CWs of the liquid surface is given by

$$P_T(Q,\omega) = \frac{k_B T Q}{\pi\rho\omega}\,\mathrm{Im}\left[\frac{1}{D(Q,\omega)}\right]. \tag{7}$$

Although the experimental dispersion relation is often deduced from the peak position ω_m of $P_T(Q,\omega)$, this gives only approximate results, because ω_m differs from the pole of $1/D(Q,\omega)$ owing to the damping [20]. This can be clearly seen in Fig. 1, where dimensionless peak position $\tilde{\omega}_m(>0)$ and dimensionless width (half width at half maximum) $\tilde{\Gamma}_h$ of Eq. (7) is plotted against $\tilde{Q}$ by dotted lines. At variance with $\tilde{\omega}_0$, $\tilde{\omega}_m$ vanishes to zero at $\tilde{Q} \approx 3.20$.

III. EXPERIMENT

Figure 2 shows an experimental setup for the surface DLS measurements schematically. The six IL samples, [C_4mim][TFSI], [TMPA][TFSI], [PP13][TFSI], and [$C_n$mim][PF_6]($n=4,6,8$), were purchased from Kanto Chemical Co. Inc. The liquid sample was enclosed in a fused-quartz cell with a diameter of 50 mm. The cell was surrounded with aluminum blocks in which a heater was embedded.

Before the DLS measurements, the sample was kept at 333 K under vacuum for about 12 h to eliminate adsorbed water. The cell was evacuated using a vacuum pump and a liquid nitrogen trap, and the measurements were performed under vacuum conditions.

We used a He-Ne laser (1.5 mW, wavelength $\lambda = 632.8$ nm) as a light source for the DLS measurement. The light scattered by the CWs was collimated by a pinhole (0.5 mm in diameter) and introduced to a photomultiplier detector through an optical fiber. The scattering wave vector Q was related to the position of the pinhole relative to the specularly reflected beam. All the optical components were mounted on an optical bench with air springs to isolate from external vibrations.

The DLS measurements were carried out in the Q range of 300 $\mathrm{cm}^{-1} < Q < 900$ cm^{-1} and at various temperature conditions. Together with the scattering from the liquid surface, the light scattered from the surfaces of optical elements was

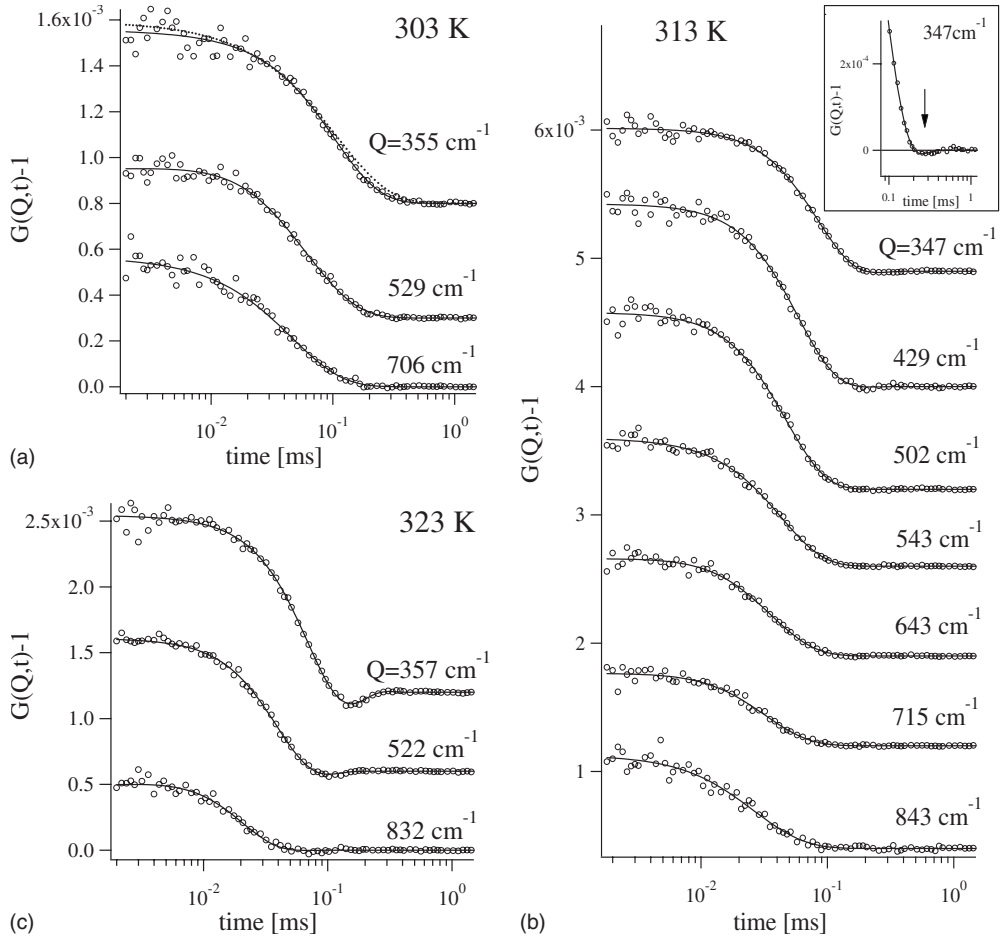

FIG. 3. Representative results of the observed and baseline-subtracted autocorrelation function $G(Q,t)-1$ for [TMPA][TFSI] at (a) 303 K, (b) 313 K, and (c) 323 K. The solid lines are the fitting curves by Eq. (8) in the oscillating regime or Eq. (10) in the overdamped regime. The dotted line in (a) $Q=355$ cm^{-1} is the fitting curve by the single exponential form Eq. (9).

optically mixed at the detector passed through the pinhole B [21]. The latter acts as the reference light or the local oscillator to fulfill the necessary conditions for optical heterodyning. From the output signal of the detector, $I(Q,t)$, the time-autocorrelation function $G(Q,t)=\langle I(Q,t)I(Q,0)\rangle/\langle I\rangle^2$ was obtained with a multiple-tau digital autocorrelator ALV-6010/160, whose minimum sampling time was 6.25 ns. Although the autocorrelation function $G(Q,t)$ can be expressed as a combination of heterodyne and homodyne terms in general [22], the heterodyne term was dominant in the present case because the reference signal is far more intense compared to the scattering from the CW. Therefore, in the following analysis, we can safely ignore the homodyne contribution. The effects of bulk scattering were also negligible, because the investigated length scale (~longer than 60 μm, deduced from the measured Q range) was sufficiently larger than the length of the fluctuations in bulk ILs. To verify the validity of the experimental method and the heterodyne analysis, we performed a measurement with water as a standard sample, in which we obtained the surface tension and the viscosity with accuracy of 1%.

Since the density of [TMPA][TFSI] was not available in the literature to our knowledge, we measured it by ourselves using a homemade dilatometer that has the same shape as a thermometer. The dilatometer was calibrated using [C_4mim][TFSI] as a standard sample.

IV. RESULTS AND DISCUSSION

A. Empirical dispersion relation for [TMPA][TFSI]

In this subsection, we empirically analyze the CW spectra in the time domain, and present the dispersion relation of the CWs. The baseline-subtracted autocorrelation functions of $G(Q,t)-1$ for [TMPA][TFSI] at 303, 313, and 323 K, at various wave vectors Q are shown in Fig. 3 as representative data for the transition between oscillating and overdamped behavior. The data points of $G(Q,t)-1$ are more scattered in the short time region because they have larger statistical errors due to the short accumulation time. At 303 K, $G(Q,t)-1$ in the whole measured Q range monotonically decreases with t except for the small t region where the data are scattered. At 323 K, $G(Q,t)-1$ in the whole measured Q range shows oscillating behavior. These results indicate the occurrence of the transition from overdamped to oscillating behavior between 303 and 323 K. At the intermediate temperature, 313 K, $G(Q,t)-1$ shows either oscillating or overdamped behavior depending on Q. At $Q=347$ cm^{-1}, the minimum of

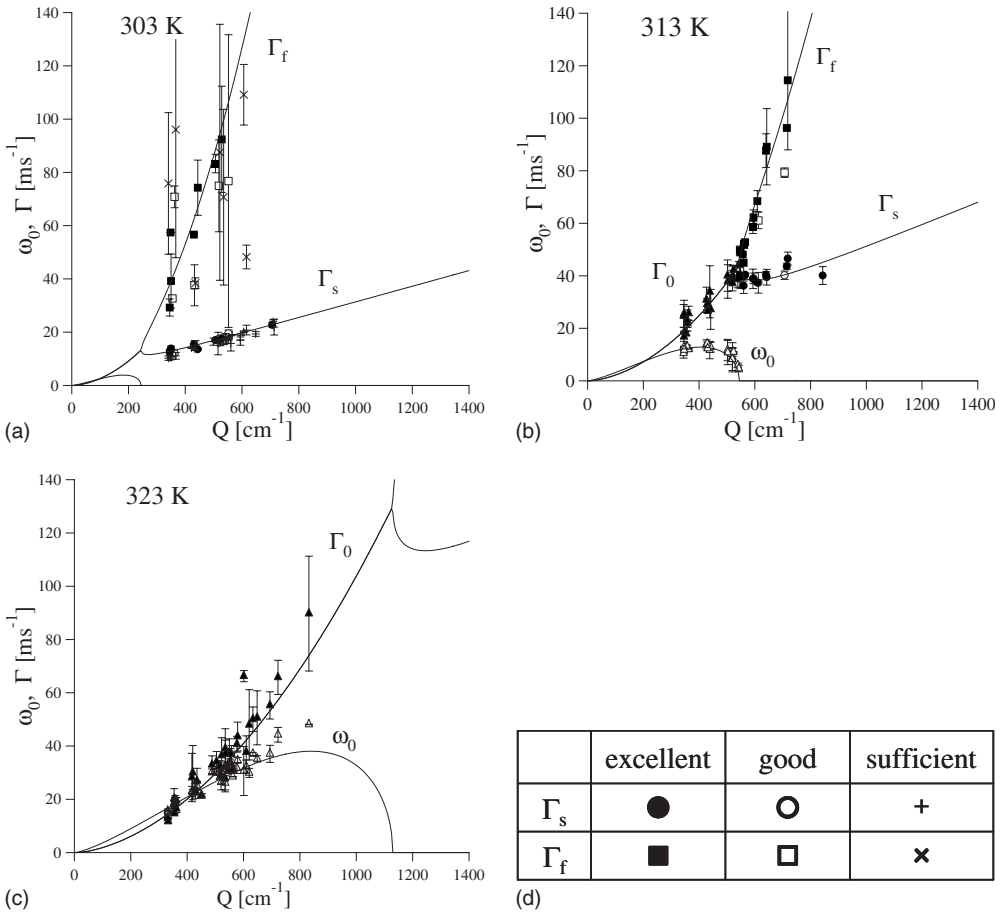

FIG. 4. Q dependence of the frequency ω_0 (△) and the damping constants Γ_0 (▲), Γ_s (●, ○, +), and Γ_f (■, □, ×) for [TMPA][TFSI] at (a) 303 K, (b) 313 K, and (c) 323 K. The symbols of overdamped coefficients are classified according to the quality of fitting, namely "excellent" (solid symbol), "good" (open symbol), and "sufficient" (cross). Criteria for qualification are described in Sec. IV A. The solid lines are the dispersion curves calculated from Eq. (6) with the parameters in Table I. The error bars are estimated by taking account of the statistical errors.

$G(Q,t)-1$ is shown at $t \approx 0.3$ ms, as shown in the inset of Fig. 3(b), indicating oscillating behavior. At $Q=843$ cm^{-1}, on the other hand, $G(Q,t)-1$ shows typical overdamped behavior, implying the occurrence of a transition from oscillating to overdamped behavior between $Q=347$ cm^{-1} and $Q=843$ cm^{-1}.

The autocorrelation functions $G(Q,t)-1$ at 323 K, which show typical oscillating behavior, are well fitted by a damped oscillating form,

$$G(Q,t) - 1 = A\cos(\omega_0 t + \phi)\exp(-\Gamma_0 t) + (\text{base line}), \quad (8)$$

as shown by the solid lines in Fig. 3(c). Here the phase term ϕ largely accounts for deviations from an exact Lorentzian form [23]. At 303 K, the autocorrelation functions show typical overdamped behavior. However, $G(Q,t)-1$ are not well fitted by Eq. (8) with $\omega_0=0$, namely a single exponential form,

$$G(Q,t) - 1 = A\exp(-\Gamma_0 t) + (\text{base line}), \quad (9)$$

as exemplified by the dotted line shown in Fig. 3(a) at $Q=355$ cm^{-1}. Instead, we found that the double exponential form

$$G(Q,t) - 1 = A\exp(-\Gamma_s t) + B\exp(-\Gamma_f t) + (\text{base line}) \quad (10)$$

with $\Gamma_s < \Gamma_f$ fits the observed data well, as depicted by solid lines in Fig. 3(a). The physical meanings of this equation will be discussed later. The base lines of $G(Q,t)-1$ vary little with t compared to $G(Q,t)-1$ (typically $\sim 1/150$). To make sure that the homodyne contribution is negligible ($\leqslant 1/100$), we analyzed all the $G(Q,t)-1$ data and derived the dispersion relations for them with and without the homodyne parts, and found no significant difference.

At the intermediate temperature of 313 K, $G(Q,t)-1$ at $Q=347$ cm^{-1} is fitted well by the damped oscillating form of Eq. (8) as shown by a solid line in Fig. 3(b), and $\omega_0=12.1$ ms^{-1} and $\Gamma_0=19.1$ ms^{-1} are obtained. The validity of Eq. (8) is also confirmed for $Q=429$, 502, and 543 cm^{-1} and the parameters are plotted in Fig. 4(b). Remarkably, ω_0 decreases above $Q=500$ cm^{-1} and vanishes to zero at $Q \approx 550$ cm^{-1}, implying that the behavior of $G(Q,t)-1$ changes from oscillating to overdamped. At Q larger than 550 cm^{-1}, Eq. (10) fits the data better than Eq. (8), as can be confirmed by the residual sum of squares. Thus the transition

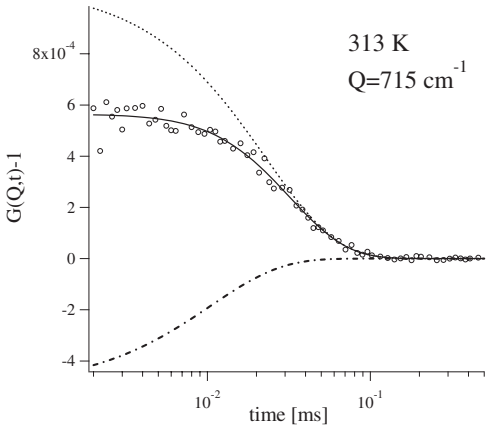

FIG. 5. The baseline-subtracted $G(Q,t)-1$ at 313 K and $Q=715\ \mathrm{cm}^{-1}$ for [TMPA][TFSI] as a representative overdamped pattern. The open circles are the experimental data, and the solid line is the fitting curve with Eq. (10). The two overdamped modes are shown separately. The slow overdamped mode is drawn by a dotted line, and the fast one is drawn by a dashed-dotted line.

from oscillating to overdamped behavior is also certified with increasing Q even at constant temperature.

Figure 5 shows the representative overdamped $G(Q,t)-1$ obtained by the experiment in the vicinity of the transition. The solid line represents the fitting curve expressed by Eq. (10), and the dotted line and the dashed-dotted line represent the slower component and the faster component, respectively. Note that $A>0$ but $B<0$ [see Eq. (12) for details].

All the empirical dispersion relations obtained for [TMPA][TFSI] using Eqs. (8) or (10) are plotted by various symbols in Fig. 4 at 303 K (a), 313 K (b), and 323 K (c). In the overdamped regime, the symbols are classified according to the quality of fitting, namely "excellent" data are plotted by solid symbols, "good" data are plotted by open symbols, and "sufficient" data are plotted by crosses. The better the fitting quality is, the more systematic Q dependence emerges. The criteria of classification will be described later.

The features of the empirical dispersion relations are summarized as follows. All the data taken at 303 K indicate overdamped behavior. The two coefficients, Γ_s and Γ_f, increase with Q, and the increasing rate of Γ_f with Q is much larger than that of Γ_s. At 313 K, ω_0 is finite for $Q<550\ \mathrm{cm}^{-1}$, but vanishes to zero for $Q\geqslant 550\ \mathrm{cm}^{-1}$ where the damping coefficient bifurcates into a faster and a slower branch. The error bars of Γ_f at 313 K become longer in the large Q range because the contribution of the fast overdamped modes become small far from the transition point from ocillating to overdamped behavior, probably the same for Γ_f at 303 K. At 323 K where $G(Q,t)-1$ behaves oscillatory, ω_0 and Γ_0 increase with Q for $Q<832\ \mathrm{cm}^{-1}$.

Let us discuss the time domain analysis in more detail. Since a time-correlation function such as $G(Q,t)$ is independent of the choice of time origin and invariant under time translation [24], it follows that

$$\left.\frac{\partial G(Q,t)}{\partial t}\right|_{t=0}=0. \tag{11}$$

Applying Eq. (11) to Eq. (10), we can obtain

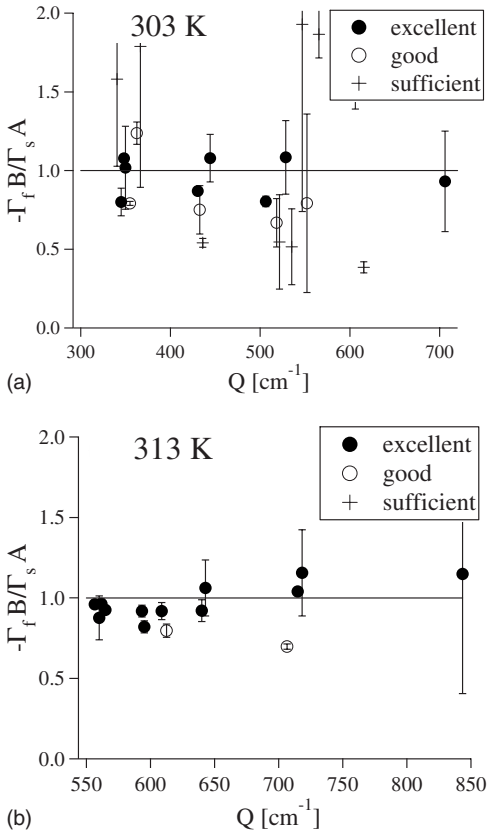

FIG. 6. $R\equiv-\Gamma_f B/\Gamma_s A$ for [TMPA][TFSI] at (a) 303 K and (b) 313 K are plotted against Q. The symbols are classified by the deviation from expected value. "Excellent" data (i.e., $|R-1|\leqslant 0.2$) are plotted by solid circles, "good" data (i.e., $0.2<|R-1|\leqslant 0.4$) are plotted by open circles, and "sufficient" data (i.e., $|R-1|>0.4$) are plotted by crosses. The error bars correspond to those in Fig. 4.

$$-\frac{\Gamma_f B}{\Gamma_s A}=1. \tag{12}$$

Although Eq. (12) tells that the four parameters (Γ_s, Γ_f, A, and B) are not independent, we have treated them as free parameters in the present analysis, and checked the consistency with Eq. (12) after the fitting procedure, as depicted in Fig. 6 where the resulting $-\Gamma_f B/\Gamma_s A(\equiv R)$ is plotted as a function of Q. At 313 K, the R values lie approximately along the straight line (i.e., $-\Gamma_f B/\Gamma_s A=1$), while at 303 K the points are more dispersed. Thus we have classified the overdamped data according to the fitting quality into three categories: "excellent" when $|R-1|\leqslant 0.2$, "good" when $0.2<|R-1|\leqslant 0.4$, and "sufficient" when $|R-1|>0.4$. The same classification was applied to Fig. 4. As already mentioned, "excellent" data provide nice dispersion curves. As the difference between Γ_s and Γ_f increases, the fitting quality is no longer "excellent" because B becomes far smaller than A.

Since Eq. (11) is general, it can be also applied to Eq. (8), leading to a relation $\tan(\phi)=-\Gamma_0/\omega_0$. We have checked that the oscillating data $G(Q,t)-1$ at 313 K are consistent with this relation almost everywhere [25]. The invalidity of Eq. (9) can be understood easily, because Eq. (11) is not satisfied by this equation.

TABLE I. Specific values of surface tension σ, viscosity η, and density ρ, which are assigned to Eq. (6) to draw the theoretical dispersion relations shown in Figs. 4 and 7.

Ionic liquid	Temperature /K	σ /mN m^{-1} *	η /mPa s *	ρ /g cm^{-3}
[TMPA][TFSI]	303	35.2 ±0.1	59.5 ±0.3	1.43 †
[TMPA][TFSI]	313	34.6 ±0.1	39.4 ±0.1	1.42 †
[TMPA][TFSI]	323	34.0 ±0.3	26.9 ±0.3	1.41 †
[C_4mim][TFSI]	303	33.5 ±0.4	37.7 ±0.2	1.43 [28]
[PP13][TFSI]	328	33.0 ±0.2	36.5 ±1.0	1.38 [29]
[C_4mim][PF_6]	333	41.3 ±0.3	47.5 ±0.4	1.34 [28]
[C_6mim][PF_6]	353	35.1 ±0.3	35.1 ±0.2	1.26 [31]
[C_8mim][PF_6]	363	29.8 ±0.6	31.4 ±0.7	1.19 [30]

[a]σ and η for all ILs are obtained by fitting the power spectrum as described in Sec. IV B.
[b]Present data.
Shaded data: transition region.

B. Theoretical dispersion relation for [TMPA][TFSI]

The theoretical dispersion relation can be calculated from Eq. (6), once numerical values of σ, η, and ρ are given. In the present work, we determined σ and η from the power spectra deduced from the present DLS experiments. This method is based on the fluctuation-dissipation theorem and the computational procedure was developed by Ohmasa *et al.* in the previous work [13], where it is confirmed that σ and η for [C_4mim][TFSI] derived by this method agree with those deduced from conventional measurements.

The theoretical expression of the power spectrum $P_T(Q,\omega)$ is given by Eq. (7). Taking into account the instrumental Q-resolution function with the standard deviation β,

$$\rho(Q,Q') = \frac{1}{\sqrt{\pi}\beta} \exp[-(Q'-Q)^2/\beta^2], \tag{13}$$

we can write the effective power spectrum $P(Q,\omega)$ in the form

$$P(Q,\omega) = \int dQ' \rho(Q,Q') P_T(Q',\omega). \tag{14}$$

In the present experimental setup, β is estimated to be ~ 48 cm^{-1}, which is compatible with the pinhole diameter. For acquisition of σ and η, we adopted a global fitting procedure. Namely, for each temperature condition, about 40 spectra taken at various Q positions are fitted by the theoretical $P(Q,\omega)$ simultaneously while sharing the same fitting parameters between these data sets.

The specific values of σ, η, and ρ for [TMPA][TFSI] are shown in Table I. The present σ values show good agreement with those obtained by a du Nouy method in our laboratory [26], and the present η show good agreement with those measured with a commercial viscometer [27]. The results of σ and η in a wide temperature range obtained by the DLS measurements will be published elsewhere [26].

In Fig. 4, the solid lines denote the theoretical dispersion curves, which reproduce the experimental dispersion relations, especially "excellent" data, very well not only in the overdamped or oscillating regime but also in the crossover region. It is of considerable significance that, starting from experimental DLS data, we have obtained nearly identical dispersion relations via two completely different routes of analysis: one is an empirical time domain analysis and the other is a theoretical frequency domain analysis. It should be noted that, although the peak position ω_m alone cannot give an accurate dispersion relation, as seen in Fig. 1, the analysis utilizing the whole power spectrum provides correct dispersion curves.

C. Dispersion relations for various ionic liquids

In the preceding subsection we have demonstrated that the experimental dispersion relations of CW spectra for [TMPA][TFSI] are well expressed by the hydrodynamic equation [Eq. (6)]. It is extremely interesting to elucidate whether this is also true for other ILs, because ILs are "designable" in a sense that the physical properties can be controlled systematically by exchanging cations and anions. Thus we have investigated the CWs spectra on the five ILs, [C_4mim][TFSI], [PP13][TFSI], and [$C_n$mim][PF_6] ($n=4,6,8$).

Figure 7 shows the dispersion relations for each ILs at the specific temperature where the transition from oscillating to overdamped behavior was observed most clearly. Namely, at 303 K for [C_4mim][TFSI], at 328 K for [PP13][TFSI], at 333 K for [C_4mim][PF_6], at 353 K for [C_6mim][PF_6], and at 363 K for [C_8mim][PF_6]. In the insets, the R values ($=-\Gamma_f B/\Gamma_s A$) are plotted against Q to show the quality of fitting. For all these ILs, overdamped behavior was observed at the lower temperatures and oscillating behavior at the higher temperatures in the whole measured Q range, which is similar to the results shown in Fig. 4 for [TMPA][TFSI].

The lines in Fig. 7 are theoretical dispersion relations, for which σ and η are obtained by fitting the power spectrum, as described in the previous subsection, and ρ are taken from the literature [28–31]. These values are listed in Table I, together with those for [TMPA][TFSI]. The present data of σ and η are in good agreement with those measured by conventional methods [28,31,32]. The data of σ and η in a wider temperature range will be published elsewhere [26], in which detailed comparison with other experimental data are also made. Overall agreements between the empirical dispersion relations and the theoretical ones are very good, indicating that, within the measured Q range, the CWs on ILs could have universal hydrodynamic properties.

One may recognize from Table I that, when the transition from oscillating to overdamped behavior takes place, the viscosity η is in the range of 40 ± 10 mPa s. In contrast, other quantities such as σ and ρ have no clear correlation with the occurrence of transition. Hence the viscosity may be regarded as the most relevant quantity for the oscillating-to-overdamped transition, which is consistent with Eq. (5) where η has the strongest dependence on $\tilde{Q}$. Since η of most ILs changes drastically with temperature following the Vogel-Fulcher-Tamman equation [33–35], one could predict the transition temperature for various other ILs without DLS experiments as long as the ILs have universal hydrodynamic properties.

An intriguing open question is to what extent the CWs on ILs keep universal hydrodynamic properties. Although no

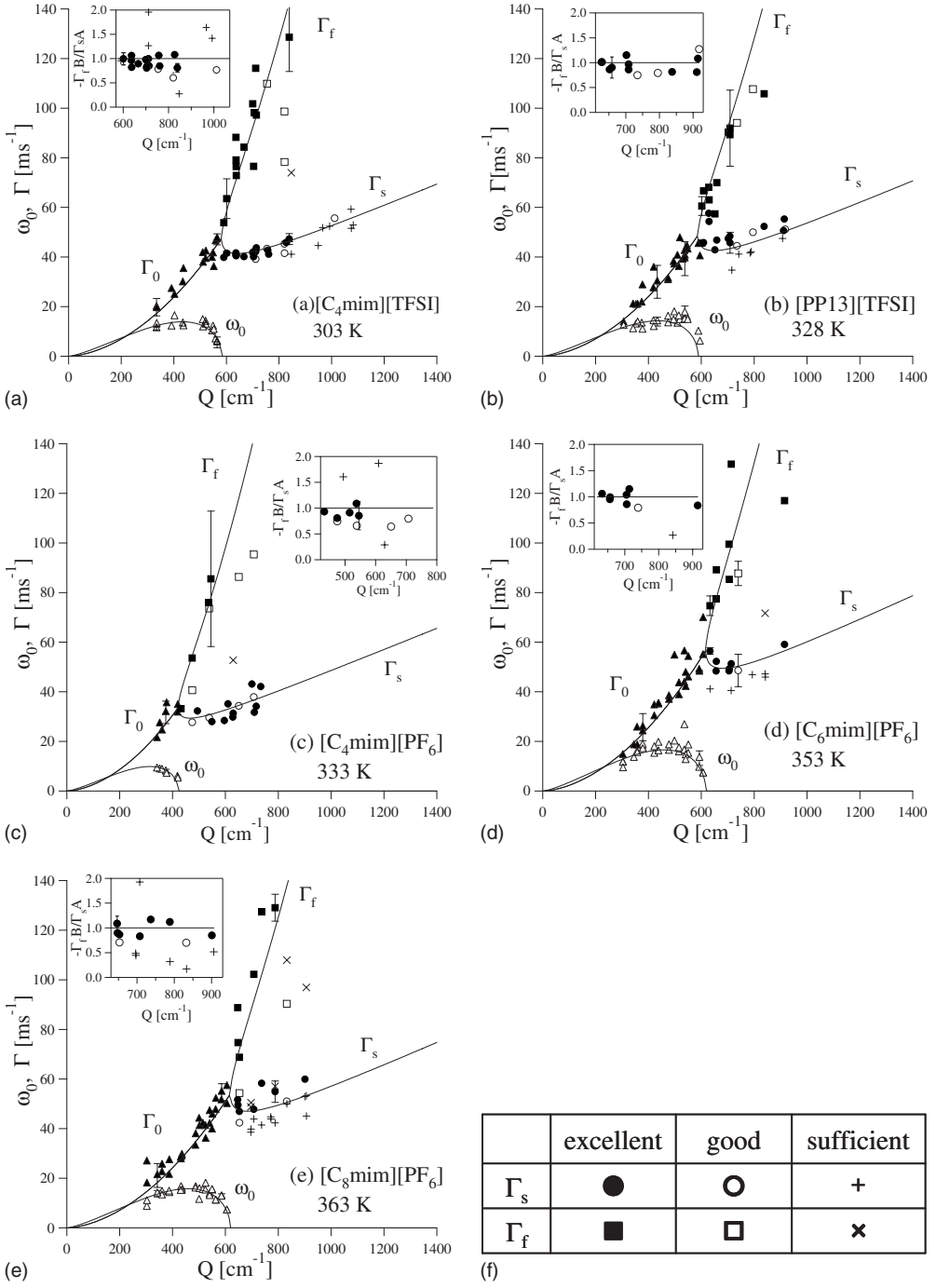

FIG. 7. Q dependence of the frequency ω_0 (▲) and the damping constants Γ_0 (▲), Γ_s (●, ○, +), and Γ_f (■, □, ×) for (a) [C_4mim][TFSI] at 303 K, (b) [PP13][TFSI] at 328 K, (c) [C_4mim][PF_6] at 323 K, (d) [C_6mim][PF_6] at 353 K, and (e) [C_8mim][PF_6] at 363 K. The solid lines are the dispersion curves calculated from Eq. (6) with the parameters in Table I. Inset: $R \equiv -\Gamma_f B/\Gamma_s A$ are plotted against Q. The symbols are classified by the deviation from expected value. "Excellent" data (i.e., $|R-1| \leq 0.2$) are plotted by solid circles, "good" data (i.e., $0.2 < |R-1| \leq 0.4$) are plotted by open circles, and "sufficient" data (i.e., $|R-1| > 0.4$) are plotted by crosses. For avoiding a too complicated drawing, only typical error bars are depicted.

significant deviation from Newtonian fluids is observed in this paper, non-Newtonian behavior is evidenced for bulk ILs with long alkyl chains by ultrasonic spectroscopy [36]. At such high frequencies ($\geq$10 MHz) and at low temperatures, CWs on ILs would exhibit non-Newtonian behavior. Moreover, CWs at large wave vectors, comparable with the inverse of molecular dimension, are particularly interesting [37,38].

V. CONCLUSION

We have measured the CW spectra on the surface of six ILs, [TMPA][TFSI], [C_4mim][TFSI], [PP13][TFSI], and

$[C_n\text{mim}][PF_6]$ ($n=4,6,8$) using DLS in the Q range from 300 to 900 cm^{-1}, and performed the fitting analysis of the spectra in the time domain to obtain the dispersion relation. The transition from oscillating to overdamped behavior was clearly found for all the ILs by adjusting the temperature. In particular, the fast overdamped modes were observed on the free liquid surface. The empirical dispersion relations agree with the theoretical dispersion relations deduced from the linearized Navier-Stokes equation to which experimentally determined density, viscosity, and surface tension are assigned.

ACKNOWLEDGMENT

This work was partially supported by the Grant-in-Aid for Scientific Research on Priority Area "Soft matter Physics" and "Science of Ionic Liquids" from Ministry of Education, Culture, Sports, Science and Technology (MEXT), and Grant-in-Aid for the global COE program "The Next Generation of Physics, Spun from Universality and Emergence" from MEXT. One of the authors (Y.O.) is also indebted to a Grant-in-Aid for Scientific Research (20540396) from MEXT. The authors thank Dr. Y. Hiejima for measuring the viscosity for [TMPA][TFSI].

[1] V. G. Levich, *Physicochemical Hydrodynamics* (Prentice-Hall, Englewood Cliffs, NJ, 1962).
[2] D. Byrne and J. C. Earnshaw, J. Phys. D **12**, 1133 (1979).
[3] A. Madsen, T. Seydel, M. Sprung, C. Gutt, M. Tolan, and G. Grubel, Phys. Rev. Lett. **92**, 096104 (2004).
[4] J. F. Crilly and J. C. Earnshaw, Biophys. J. **41**, 197 (1983).
[5] T. Welton, Chem. Rev. (Washington, D.C.) **99**, 2071 (1999).
[6] R. T. Carlin, H. C. De Long, J. Fuller, and P. C. Trulove, J. Electrochem. Soc. **141**, L73 (1994).
[7] P. Wang, S. M. Zakeeruddin, J. E. Moser, and M. Gratzel, J. Phys. Chem. B **107**, 13280 (2003).
[8] E. Sloutskin, B. M. Ocko, L. Tamam, I. Kuzmenko, T. Gog, and M. Deutsch, J. Am. Chem. Soc. **127**, 7796 (2005).
[9] T. Iimori, T. Iwahashi, K. Kanai, K. Seki, J. Sung, D. Kim, H. Hamaguchi, and Y. Ouchi, J. Phys. Chem. B **111**, 4860 (2007).
[10] C. S. Santos and S. Baldelli, J. Phys. Chem. B **111**, 4715 (2007).
[11] G. Law, P. R. Watson, A. J. Carmichael, and K. R. Seddon, Phys. Chem. Chem. Phys. **3**, 2879 (2001).
[12] R. M. Lynden-Bell and M. Del Popolo, Phys. Chem. Chem. Phys. **8**, 949 (2006).
[13] Y. Ohmasa, T. Hoshino, R. Osada, and M. Yao, Chem. Phys. Lett. **455**, 184 (2008).
[14] E. Sloutskin, P. Huber, M. Wolff, B. M. Ocko, A. Madsen, M. Sprung, V. Schön, J. Baumert, and M. Deutsch, Phys. Rev. E **77**, 060601(R) (2008).
[15] V. Halka, R. Tsekov, and W. Freyland, Phys. Chem. Chem. Phys. **7**, 2038 (2005).
[16] V. Halka, R. Tsekov, and W. Freyland, J. Phys.: Condens. Matter **17**, S3325 (2005).
[17] V. Halka, R. Tsekov, I. Mechdiev, and W. Freyland, Z. Phys. Chem. (Munich) **221**, 549 (2007).
[18] M. A. Bouchiat and J. Meunier, J. Phys. (Paris) **32**, 561 (1971).
[19] J. Jäckle and K. Kawasaki, J. Phys.: Condens. Matter **7**, 4351 (1995).
[20] *Light Scattering by Liquid Surfaces and Complementary Techniques*, edited by D. Langevin (Dekker, New York, 1992), Chap. 7.
[21] *Light Scattering by Liquid Surfaces and Complementary Techniques* (Ref. [20]), Chap. 5.
[22] B. J. Berne and R. Pecora, *Dynamic Light Scattering* (Wiley, New York, 1976).
[23] J. C. Earnshaw and R. C. McGivern, J. Phys. D **20**, 82 (1987).
[24] J. P. Hansen and I. R. McDonald, *Theory of Simple Liquids* (Academic Press, London, 1986).
[25] T. Hoshino, Ph.D. thesis, Kyoto University, Kyoto, 2009.
[26] R. Osada *et al.* (unpublished).
[27] Y. Hiejima (private communication).
[28] H. Tokuda, K. Hayamizu, K. Ishii, M. A. B. H. Susan, and M. Watanabe, J. Phys. Chem. B **108**, 16593 (2004).
[29] Ramesh L. Gardas, Henrique F. Costa, Mara G. Freire, Pedro J. Carvalho, Isabel M. Marrucho, Isabel M. A. Fonseca, Abel G. M. Ferreira, and João A. P. Coutinho, J. Chem. Eng. Data **53**, 805 (2008).
[30] K. R. Harris, M. Kanakubo, and L. A. Woolf, J. Chem. Eng. Data **51**, 1161 (2006).
[31] K. R. Harris, M. Kanakubo, and L. A. Woolf, J. Chem. Eng. Data **52**, 1080 (2007).
[32] Mara G. Freire, Pedro J. Carvalho, Ana M. Fernandes, Isabel M. Marrucho, António J. Queimada, and João A. P. Coutinho, J. Colloid Interface Sci. **314**, 621 (2007).
[33] H. Vogel, Phys. Z. **22**, 645 (1921).
[34] G. S. Fulcher, J. Am. Ceram. Soc. **8**, 339 (1923).
[35] G. Tamman and W. Hasse, Z. Anorg. Allg. Chem. **156**, 245 (1926).
[36] W. Makino, R. Kishikawa, M. Mizoshiri, S. Takeda, and M. Yao, J. Chem. Phys. **129**, 104510 (2008).
[37] K. R. Mecke and S. Dietrich, Phys. Rev. E **59**, 6766 (1999).
[38] P. Tarazona, R. Checa, and E. Chacón, Phys. Rev. Lett. **99**, 196101 (2007).